Exclusive Study of Deuteron Electrodisintegration near Threshold

(December 3, 2001)

G.D. Cates, R. Lindgren, N. Liyanage, B. E. Norum (Spokesman),
B. Sawatzky, L.C. Smith, and K. Wang (Spokesman, Contact)
University of Virginia, Charlottesville, VA

H. Kanda, K. Kino, K. Maeda, and T. Tamae (Spokesman)
Tohoku University, Sendai, Japan

W. Bertozzi (Spokesman), S. Gilad, S. Sirca, Z.-L. Zhou
MIT, Cambridge, MA

H. Arenhövel
University of Mainz, Mainz, Germany

T. Suda
RIKEN, Wako, Japan

T. Kobayashi
Teikyo University, Tokyo, Japan

R. Igarashi, N. Kolb, R. Pywell
University of Saskatchewan, Saskatoon, Canada

A. Hotta
University of Massachusetts, Amherst, MA

J.R.M. Annand, D. Ireland, J. Kellie, K. Livingston
G. Rosner, D. Watt *University of Glasgow, Glasgow, Scotland, UK*

X. Jiang
Rutgers University, New Brunswick, NJ

J. P. Chen, D. W. Higinbotham
Jefferson Laboratory, Newport News, VA

V. Nelyubin
St. Petersburg Nuclear Physics Inst., Gatchina, Russia

Abstract

Elastic electron scattering from the deuteron and near-threshold electrodisintegration have long provided benchmarks against which models of the nucleon-nucleon interaction are measured. Recent measurements of T_{20} in elastic scattering have tightened the constraints but still leave room for ambiguity. We propose to make similar improvements in the constraints imposed by electrodisintegration by making an exclusive study of the reaction $d(\vec{e}, e'p)n$ at $Q^2 = 12$ fm^{-2} and $E_{np} = 2$, 4, 6, 8 MeV. Under these kinematics, non-nucleonic as well as nucleonic degrees of freedom and relativistic effects are expected to play major roles. The experiment will be conducted in Hall A at JLab using the polarized CW electron beam, an HRS spectrometer to detect the electron, and the BigBite spectrometer to detect the proton. Near threshold the large momentum and angular (in both the horizontal and vertical planes) acceptances of the BigBite spectrometer will permit most of the allowed phase space of the proton to be measured in a single setting. The large acceptance of the BigBite spectrometer will enable us to detect simultaneously deuterons from elastic scattering over the same range of Q^2. The first part of the experiment will be to extract the structure functions f_{LT}, f_{TT}, and f'_{LT} from the ϕ_p dependence of the cross section measured with an electron beam energy of 3200 MeV and electron scattering angle of 12.5°. The second part of the experiment will be to separate the longitudinal and transverse structure functions, f_L and f_T, by performing complementary measurements with a beam energy of 550 MeV and electron scattering angle of 90°. The individual structure functions are expected to be particularly sensitive to different components of the reaction mechanism. For example, f_{LT} is expected to be sensitive to relativistic effects, f_T is expected to be dominated by MEC effects, and f'_{LT} vanishes unless final state interactions are present and is expected to be insensitive to non-nucleonic degrees of freedom. The longitudinal cross section for elastic scattering depends on the isoscalar charge current whereas f_L for electrodisintegration depends on the isovector charge current as well. Comparison of the two, as measured at the same time will allow us to separate the two contributions. A comparison of these data with relativistic model calculations will, within the context of each model, isolate and test individual interactions providing a more stringent test of model calculations.

1 Introduction

The defining goal of nuclear physics is to understand the composition and dynamics of nuclei in terms of their constituents. A first step towards this goal is to understand the interaction between nucleons. As the only stable, two-nucleon configuration the deuteron is the ideal place to probe this interaction and to test our understanding of it. Electrodisintegration is an excellent way to investigate the system for several reasons. First, the interaction mechanism is well-understood and weak. Second, in comparison to photodisintegration which occurs at a single four-momentum transfer ($Q^2 = 0$), electrodisintegration provides a distribution over Q^2. By scanning over different regions of momentum transfer, one can examine the physics important in different domains. One can get a two-dimensional picture by introducing an additional degree of freedom degree, the energy transfer, ν, of the virtual photon. By measuring electron scattering at values of Q^2 and ν corresponding to elastic scattering one measures the electromagnetic form factors of the target nucleus. By measuring at higher values of ν (electrodisintegration) one introduces dynamics into the final state which can be examined by means of coincidence measurements such as $d(\vec{e}, e'p)n$. Measurements of the coincidence structure functions provide much greater insight into the interactions of the nuclear constituents. Moreover, the dependences of these structure functions on Q^2 and the invariant mass W (or equivalently of E_{np}, the center-of-mass kinetic energy) of the final two-nucleon system can be expected to be differentially sensitive to different aspects of the physics.

Elastic electron scattering from the deuteron and near-threshold electrodisintegration have long provided benchmarks against which models of the nucleon-nucleon interaction are measured. Recent measurements of T_{20} in elastic scattering have tightened the constraints but still leave room for ambiguity. We propose to make similar improvements in the constraints imposed by electrodisintegration by making an exclusive study of the reaction $d(\vec{e}, e'p)n$ at $Q^2 = 12\,\mathrm{fm}^{-2}$ and $E_{np} = 2, 4, 6, 8$ MeV. Under these kinematics, non-nucleonic as well as nucleonic degrees of freedom and relativistic effects are expected to play major roles.

The potential significance of these studies was highlighted at the PAC14 Few-

Body Workshop [1]. There, the first of three "Key Questions" was identified as 'Can few-body systems be understood in terms of a "*standard model" for nuclear physics with only nucleon degrees-of-freedom?'* Under this the first three key issues were identified as

- Is a consistent and "exact" description of ^{2}H, ^{3}H, ^{3}He, and ^{4}He possible within a standard model? (i.e. can a single interaction and current operator account for all nuclei?)
- Precise and complete tests of the "*standard model"* need to be identified and carried out experimentally.
- A complete "*standard model"* requires correct incorporation of relativistic effects, meson-exchange currents, and isobar currents.

In looking to a program of measurements to address these issues the first item listed under "Experimental Opportunities for the Future" was *"Threshold deuteron electrodisintegration: Measurements of this reaction at Jefferson Lab could extend the exploration of the role of meson-exchange currents to higher momentum transfer."* While the current proposal does not focus on the highest momentum transfers possible, it does address directly both the nucleonic and non-nucleonic currents in the deuteron. Thus, the proposed measurements constitute the first step on this important path.

The great wealth of information available from the electrodisintegration of deuteron will be exploited. In the case of unpolarized beam and target, the coincidence cross section contains four dynamical functions, the longitudinal (f_L), transverse (f_T), transverse-transverse (f_{TT}), and the longitudinal-transverse (f_{LT}) interference terms. A fifth structure function (f'_{LT}) will be involved when a polarized electron beam is used. Earlier studies have shown the strong sensitivity of deuteron electrodisintegration to non-nucleon degrees of freedom. Therefore, it is an important step to study in detail effects like meson-exchange currents (MEC) and isobar currents (IC), as well as relativistic corrections to the structure functions. From the theoretical side, these interaction effects can be cleanly investigated in the two-nucleon system since there are no problems arising from many-particle effects. Hence, reliable calculations are possible.

Inclusive data [2] on the reaction $d(e,e')pn$ near threshold showed that nearly 100% of the experimental cross section near $Q^2 = 12\,fm^{-2}$ can be accounted for by the inclusion of MEC's. While this established that non-nucleonic degrees of freedom are important, the availability of only cross section data limits the interpretive and thus predictive power of the calculations. The MEC's are expected to be particularly important to the transverse structure function f_T so extracting f_T will be one of the most important foci of the proposed work. A precise determination of f_T as a function of θ_p, the angle at which the proton emerges in the center of mass system, and E_{np} will place tight constraints on models of non-nucleonic effects.

The structure function f_T will be extracted via a Rosenbluth separation so, necessarily, we will extract f_L as well. The function f_L is insensitive to MEC's so should provide us with an opportunity to study the isovector charge contribution.

It was found from theoretical calculations [3] [4] and from data [5] [6] [7] that the longitudinal-transverse component f_{LT} is specifically sensitive to relativistic corrections (RC). It was also shown [4] that relativistic effects become visible above $Q^2 = 5fm^{-2}$ and increase with the momentum transfer. Close to the quasi-elastic (QE) region the relativistic two-body contribution is small, but the effect increases as one moves away from QE kinematics. Since most of the previous data were obtained in the QE region and at lower Q^2, measurements near threshold and at higher Q^2 will enable us to see a sizable contribution from relativistic effects. The importance of understanding relativistic effects is clear; it will pave the way to searches for a quark-gluon signature in future investigations at higher Q^2. As well, when combined with our determination of f_L it will assist us to extract a more reliable picture of the isovector charge current. This will be the second major focus of the experiment.

Due to the azimuthal (ϕ_p) dependence of the partial cross section σ_{LT}, its contribution to the cross section was averaged to in inclusive measurements. However, the selective sensitivity of f_{LT} to RC can be exploited in an exclusive measurement. Doing so will be the third major focus of our experiment.

With the polarized electron beam, the fifth structure function f'_{LT} can be

obtained. Due to the larger vertical acceptance of the BigBite spectrometer, f'_{LT} can be measured over a wide range of E_{np} from threshold up to the region of the Δ. The function f'_{LT} vanishes in plane wave approximation, so a finite f'_{LT} will enable us to study final state interactions (FSI) if for no other reason than to account for their effects in our measurements of the other structure functions.

To date, very few measurements of either photo- or electrodisintegration of the deuteron near threshold have been made. Total, unpolarized photodisintegration cross sections for $E_\gamma \approx 2.6$ MeV [8], corresponding to $E_{np} \approx 0.4$ MeV, have been measured as have differential cross sections ($\theta_p = 0°$, $90°$, and $180°$) for $E_\gamma \approx 10$ MeV [8]. Earlier this year, a UVA/Saskatchewan/Duke collaboration measured the reaction $d(\vec{\gamma}, n)p$ at E_γ=2.6, 3.5, 4.0, and 6.0 MeV corresponding to E_{np}=0.4, 1.3, 1.8, and 3.8 MeV; these data are currently being analyzed. The electrodisintegration measurement that is closest to threshold was made at Sendai with $E_{np} \approx 18$ MeV and $Q^2 \approx 0.11$ fm^2. None of these measurements was particularly or selectively sensitive to IC, MEC, or RC.

To obtain more detailed knowledge from deuteron electrodisintegration, out-of-plane measurement of an emitted nucleon in coincidence with the scattered electron is the next step. However very few such measurements have been done due to their extreme difficulty. The cross section is typically as low as a few $nb/MeV/sr^2$ and it is almost impossible to get high quality data using a beam with a low duty factor. The CW beam at JLab and the combination of an HRS (High Resolution Spectrometer) and the BigBite spectrometer in Hall-A provide a unique facility to undertake the experiment.

The kinematics of the threshold electrodisintegration reaction are almost identical to those of elastic scattering. Thus, we will detect in the HRS electrons from elastic scattering. The very large momentum momentum acceptance of the BigBite spectrometer will enable us to measure the corresponding recoiling deuteron as well. Time-of-flight and E-dE cuts will enable us to distinguish them from protons.

We propose an out-of-plane measurement of deuteron electrodisintegration in Hall A at $Q^2 \approx 12 fm^{-2}$ near threshold (E_{np}= 2 to 8 MeV), where MEC,

IC, and RC effects are expected to be eminent and distinguishable. The Q^2 chosen corresponds to a minimum in the cross section as calculated without non-nucleonic and relativistic effects, thus enhancing relatively these latter effects. It is high enough to investigate these effects while low enough to avoid involving quark-gluon effects. The experiment consists of two parts. The data measured using E= 3200 MeV will be used to extract the three interference structure functions, f_{LT}, f_{TT}, f'_{LT}, as well as a sum of the longitudinal and the transverse cross sections. The data measured using E= 550 MeV will be used to separate the longitudinal and transverse structure functions, f_L and f_T, in combination with the data taken at E= 3200 MeV. The particular sensitivity of f_L to the isovector charge currents, that of f_T to MEC, that of f_{LT} to RC, and that of f'_{LT} to FSI will enable us to test existing models of the nucleon-nucleon interaction and firmly constrain future calculations.

2 Previous Data

Over the past forty years there have been many studies of deuteron electrodisintegration, mostly by means of inclusive measurements. Starting in 1962 [9] at $Q^2 = 0.16 fm^{-2}$ the measurements were extended to $28 fm^{-2}$ in 1985 [2] and to $40 fm^{-2}$ in 1991 [10] [11]. The high Q^2 measurements were performed at backward angles and involved the interaction of transverse virtual photons with the current and magnetization densities of the deuteron. Within a few MeV of threshold, the M1 transition from the isospin singlet ${}^3S_1 + {}^3D_1$ ground state to the final scattering state, isospin triplet ${}^1S_0$, dominates the cross section. Near $Q^2 = 12 fm^{-2}$, the plane wave impulse approximation reaches a deep minimum due to the destructive interference between ${}^3S_1 \rightarrow {}^1S_0$ and ${}^3D_1 \rightarrow {}^1S_0$ transition as shown in Fig. 2 in [2]. The filling in of this dip by the inclusion of MEC constituted a major step forward in our theoretical understanding of nucleon interactions.

Coincidence measurements on the deuteron were performed at Kharkov [12] [13] and Saclay [14]. They were all in coplanar kinematics and no attempt was made to dissect the cross section. The measurement of coincidence cross sections for deuteron electrodisintegration in out-of-plane kinematics was pioneered by Tamae *et al.* at Sendai [15] for $Q^2 = 0.11 fm^{-2}$ and $E_{np} = 18 MeV$. The two interference terms and the sum of longitudinal and transverse terms were studied. The results were in good agreement with theoretical calculations based on the Paris potential. However, in that low Q^2 region, the structure functions are dominated by the conventional impulse approximation which considers only nucleonic, non-relativistic contributions to the nuclear charge and current densities. To investigate the contributions from non-nucleon degrees of freedom, one has to go higher momentum transfer, which will require higher electron beam energy and/or larger electron scattering angle.

A proposal for coplanar measurements [16] at $Q^2 = 8.7 fm^{-2}$ was approved at the MIT-Bates Laboratory. Unfortunately, due to the decommissioning of the MEPS spectrometer, the proton detector, the project was canceled. At Bonn, data for f_{LT} was obtained at $Q^2 = 4.5 fm^{-2}$ and $E_{np} = 15 MeV$ [17]. One measurement of the fifth structure function in the QE region at

$Q^2 = 3.3 fm^{-2}$ was performed at the MIT-Bates Laboratory [18], but it suffered from large uncertainties. Another measurement conducted at the MIT-Bates Laboratory with $E_e = 800$ MeV and $Q^2 = 3.8\ fm^{-2}$ [19] focused on the dip region below the Δ peak. The interference terms and the fifth structure functions were obtained, clearly revealing strong evidence for RC and FSI. There are also data sets from NIKHEF in the QE and $\Delta-$regions[20] [21].

All these data and more are summarized in Table 1. Most of these data are either near the QE or Δ regions and at lower momentum transfer. There is no uniform set of data from which all the five structure functions have been extracted, especially at higher Q^2 and near the threshold region where interaction effects are larger. Our understanding of the two-body system and the nucleon-nucleon interaction will be greatly enhanced by the availability of a complete near-threshold data set obtained under kinematics, $Q^2 = 12 fm^{-2}$, where the various components make visible contributions.

A large number of measurements of elastic electron scattering from the deuteron have been made. The two most complete data sets in the Q^2 range of interest are those of Arnold *et al.,* [30] and Auffret *et al.,* [31]. These two data sets characterize separately both the longitudinal and transverse form factors.

Lab.	Q^2 (fm^{-2})	*Region*	goal	Ref.
Kharkov	4.1	QE	p_N, $d\sigma$	[12]
Kharkov	7.2	QE	p_N	[13]
Saclay	1.66	Δ	$d\sigma$	[14]
Saclay	11	QE	L,T,LT	[22]
Sendai	0.11	thrs	L+T,LT,TT	[15]
Bonn	4.5	Δ	$d\sigma$	[23]
Bonn	3.7	QE	LT	[7]
Bonn	3.1	Δ	$d\sigma$	[17]
NIKHEF	7	QE	L,T	[24]
NIKHEF	5.4	QE	L,T,LT	[20]
NIKHEF	0.77	Δ	TT	[21]
NIKHEF	5.15	QE	LT, $d\sigma$	[6]
Bates	3.8	QE	L,T,LT	[25]
Bates	3.3	QE	LT'	[18]
Bates	3.86	Dip	LT,TT,LT'	[19]
Bates	5.15	QE	LT,TT,LT'	[26]
Mainz	9.3	QE-Δ	p_m	[27]
Mainz	2-4	Dip	L,T	[28]
SLAC	>30	QE	p_m	[29]

Table 1: Previous data from coincidence measurements of deuteron electrodisintegration, p_N and p_m represent the nucleon momentum and missing momentum respectively.

3 Scientific Motivation

3.1 Theoretical Development

Early theoretical work on exclusive deuteron electrodisintegration was carried out by Fabian and Arenhövel [32], within a non-relativistic framework including MEC and IC. The T-matrix was calculated in a multipole expansion up to L=6 (including the FSI) while for all higher multipoles the Born approximation for the final-state was used. The calculated cross sections are in good agreement with inclusive data for $0 < Q^2 < 20 fm^{-2}$.

In [33], Arenhövel reported an interpretation of the d(e,e'p) data from Saclay [34] in which FSI, MEC and IC were studied. The effects turned out to be very important except for the QE region . Taking into account these effects led to a satisfactory agreement with experiment, whereas the Born or impulse approximation failed to give even a fair description.

Laget's calculation [35] included FSI and MEC. His analysis of existing data provided strong constraints on the high momentum part of the wave function of the few-body system. The corrections to the impulse approximation are affected by gauge invariance and reproduce a wide range of data obtained under very different kinematic conditions. He emphasized that a more accurate determination requires a significant increase of the duty factor and extension of the study to higher momentum.

Relativistic aspects of the theoretical approaches were explored by Cambi, Mosconi and Ricci [36] [37]. They concluded that although relativistic corrections to the charge density in deuteron photodisintegration are important, while the effects have not been examined for electron scattering experiment yet.

Mosconi and Ricci[3] studied the effects of nucleonic and pionic relativistic corrections on the structure functions for the $d(\vec{e}, e'p)n$ reaction in the QE region. The functions f_L, f_{LT}, and f'_{LT} show remarkable variations in forward and backward directions.

Observables originating from polarized electron and polarized target were investigated by Arenhövel *et al.* [38] within a non-relativistic framework, but with lowest order relativistic contributions to the one-body current. The structure functions and the asymmetries corresponding to the various nucleon polarization components were studied with respect to their sensitivity to the potential model, subnucleonic degrees of freedom, and relativistic effects in different kinematic regions.

A through relativistic analysis of both elastic electron scattering from the deuteron and electrodisintegration of the deuteron has been performed by J. A. Tjon *et al.* [39] Their calculations are based on a relativistic covariant field theoretical Bethe-Salpeter equation approach and contain a consistent relativistic treatment of both the electromagnetic current and nucleon-nucleon interaction. Contributions from meson exchange currents including $\rho\pi\omega$ and $\omega\epsilon\gamma$ are incorporated.

Recently, a consistent treatment of relativistic effects in deuteron electrodisintegration was systematically investigated in various regions of energy and momentum transfer by Ritz *et al.* [4]. In this work the equation-of-motion and the unitarily equivalent S-matrix approaches were used. In a (p/M) expansion, all leading order relativistic $\pi-$exchange contributions consistent with the Bonn one-boson-exchange potential model are included. In addition, static heavy-meson-exchange currents including boost terms, $\gamma\pi\rho/\omega$ currents, and $\Delta-$isobar contributions were considered. Sizable effects from the various relativistic two-body contributions, mainly from $\pi-$exchange, were found in inclusive form factors and exclusive structure functions for a variety of kinematic regions. The variation of different potential models was examined and the differences found to be small.

3.2 Kinematics and Cross Section

There are two planes involved in the measurement. One is the scattering plane, defined by the momentum of the scattering electron and the incident beam axis; the other is the reaction plane, defined by the three-momenta of the virtual photon and the emitted proton, as shown in Fig. 1. The incident

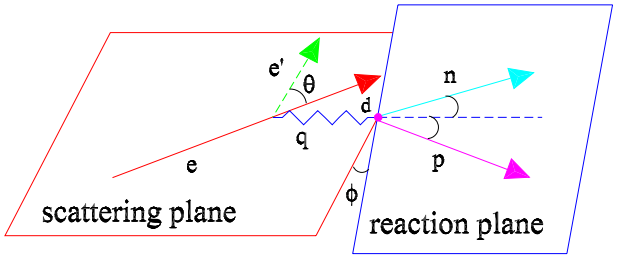

Figure 1: Schematic geometry of the deuteron disintegration reaction. In this figure the incident (scattered) electron beam energy is e (e') and the scattering angle is θ.

(scattered) electron beam energy is E (E'), and the scattering angle θ_e.

The squared four-momentum transfer q^2 carried by the virtual photon is

$$-q^2 = Q^2 = 4EE' \sin^2 \frac{\theta_e}{2},$$

Q^2 is related to the invariant mass of the final state W by

$$W^2 = 2m\nu + m^2 - Q^2,$$

where ν is the energy carried by the virtual photon, m is the mass of the deuteron and

$$\nu = E - E'.$$

The excitation energy or the relative energy of the two nucleon system after the scattering is defined as

$$E_{np} = \Delta W = W - m_p - m_n$$

where m_p and m_n are the mass of proton and neutron respectively.

According to [33], the triply differential cross section for deuteron electrodisintegration can be written as

$$\frac{d^3\sigma}{dE' d\Omega_e d\Omega_p} = C_n(\rho_L f_L + \rho_T f_T + \rho_{LT} f_{LT} \cos\phi_p + \rho_{TT} f_{TT} \cos 2\phi_p + h\rho'_{LT} f'_{LT} \sin\phi_p) \quad (1)$$

where $d\Omega_e$ is the differential solid angle subtended by the electron arm in the laboratory frame, and $d\Omega_p$ is for proton in the proton-neutron CM frame with ϕ_p the azimuthal angle of the proton relative to the virtual photon direction.

$$C_n = \frac{\alpha E'}{6\pi^2 Q^4 E},$$

where α is the fine structure constant, $f_{\lambda\lambda'}$ are nuclear structure functions, the kinematic functions $\rho_{\lambda\lambda'}$ describe the polarization density matrix of the exchanged virtual photon, and the virtual photon density matrix is given by [32]

$$\sigma^{(\gamma)}_{\mu'\mu} = \frac{\alpha}{2\pi^2}\frac{E'}{EQ^4}\rho_{\mu\mu'},$$

with $\mu = 0$ for longitudinal and $\mu = \pm 1$ for transverse polarization of the virtual photon. The ratio of ρ_L and ρ_T will be used as relative longitudinal polarization according to

$$\epsilon_L = \frac{\rho_L}{2\rho_T}. \quad (2)$$

In the above expression, f_L and f_T are the transverse and longitudinal structure functions, in principal, they can be separated by choosing two different sets of beam energy and scattering angle at fixed Q^2 and ν. The rest are the interference terms between longitudinal and transverse (f_{LT}), as well as transverse and transverse (f_{TT}). The f'_{LT} term is proportional to the helicity of the electron beam, h, and $sin\phi_p$. These interference terms are not visible in inclusive measurements, since their contribution cancels in the summation over the azimuthal angle ϕ_p. However, these terms are expected to contain new information about the N-N interaction.

The azimuthal angle dependence of the cross section can be used to separate the interference terms. While f_L, f_T and f_{LT} can, in principal, be determined

using coplanar geometry for $\phi_p = 0$ and π, f_{TT} will require an out-of-plane measurement. Similarly, in principal f'_{LT} can be measured at $\phi = 90°$ with $h = 1$ and $h = -1$. However, in order to extract these relatively small quantities with a minimal sensitivity to systematic uncertainties one must perform a measurement with as much out-of-plane acceptance as possible.

Defining

$$\xi = \frac{Q^2}{q_3^2},$$

$$\eta = \tan^2 \frac{1}{2}\theta_e,$$

and

$$\beta = \frac{q_3}{q_3^c}$$

with q_3 the three-momentum of the virtual in the laboratory frame and q_3^c the three-momentum of the virtual in the center mass frame, the $\rho_{\lambda\lambda'}$ can be explicitly expressed as [32] [38]

$$\rho_L = \beta^2 \frac{Q^2\xi^2}{2\eta},$$

$$\rho_T = \frac{Q^2}{2}(1 + \frac{\xi}{2\eta}),$$

$$\rho_{LT} = \beta Q^2 \sqrt{2(\xi + \eta)} \frac{\xi}{4\eta},$$

$$\rho_{TT} = -\frac{Q^2\xi}{4\eta},$$

$$\rho'_{LT} = \beta \frac{Q^2\xi}{2\sqrt{2\eta}}.$$

3.3 Theoretical Predictions

The aforementioned calculations as well as others not listed give reasonable descriptions of the inclusive cross sections in this range of momentum transfer

that have been measured to date. They are all untested at the level of detail that will be made possible by the proposed measurements. For the purpose of illustrating the sensitivities of the various observables to the components of the underlying physics we have chosen to focus on the calculations of Arenhövel.

Figs. 2, 3 and 4 show the predictions of Arenhövel [40] for all five structure functions for E_{np} = 2, 4, and 6 MeV and $Q^2 = 12fm^{-2}$. In these figures, the dotted curves represent his "Normal" calculation which is based on the Impulse Approximation (IA) plus FSI; the dashed curves represent Normal+MEC; the dash-dot curves represent Normal+MEC+IC; and the solid represents Normal+MEC+IC+RC.

Since f_L originates with the charge density, it is not expected to be sensitive to MEC. Consequently, in the f_L panels of all three figures the dashed (Normal+MEC) curve lies atop the dotted (Normal) curve (creating a dot-long dash curve). In addition, this calculation sets a scale for the IC contribution to f_L at about 15% and that of the RC at about 6%. The calculation indicates that in our kinematics the IC and RC contributions generate a constant shift of f_L and f_T. Thus, the shape and magnitude of $f_L(\theta_p)$ can provide a sensitive test of the isovector charge current contribution prediction of calculations wherein the isoscaler charge current contribution has been constrained by the elastic scattering results.

Unlike f_L, the f_T is very sensitive to MECs. For E_{np} = 2 MeV the MECs generate about 65% of the cross section while ICs and RCs contribute about 20% and 15% respectively. By comparing f_T at different values of E_{np}, one sees that the MEC effects are larger at smaller E_{np}.

One attractive feature of f_{LT} is its selective sensitivity to the relativistic corrections. While MECs and ICs do not make a big change to f_{LT}, the relativistic corrections affect not only the amplitude but also the shape; there is even a sign change near 90°. At $\theta_p = 140°$, RCs increase f_{LT} by 45% for E_{np}=6 MeV. In contrast to the effect of MECs on f_T, the effect of RCs on f_{LT} increases as E_{np} increases.

In the kinematic region under investigation neither MECs, ICs, nor RCs are

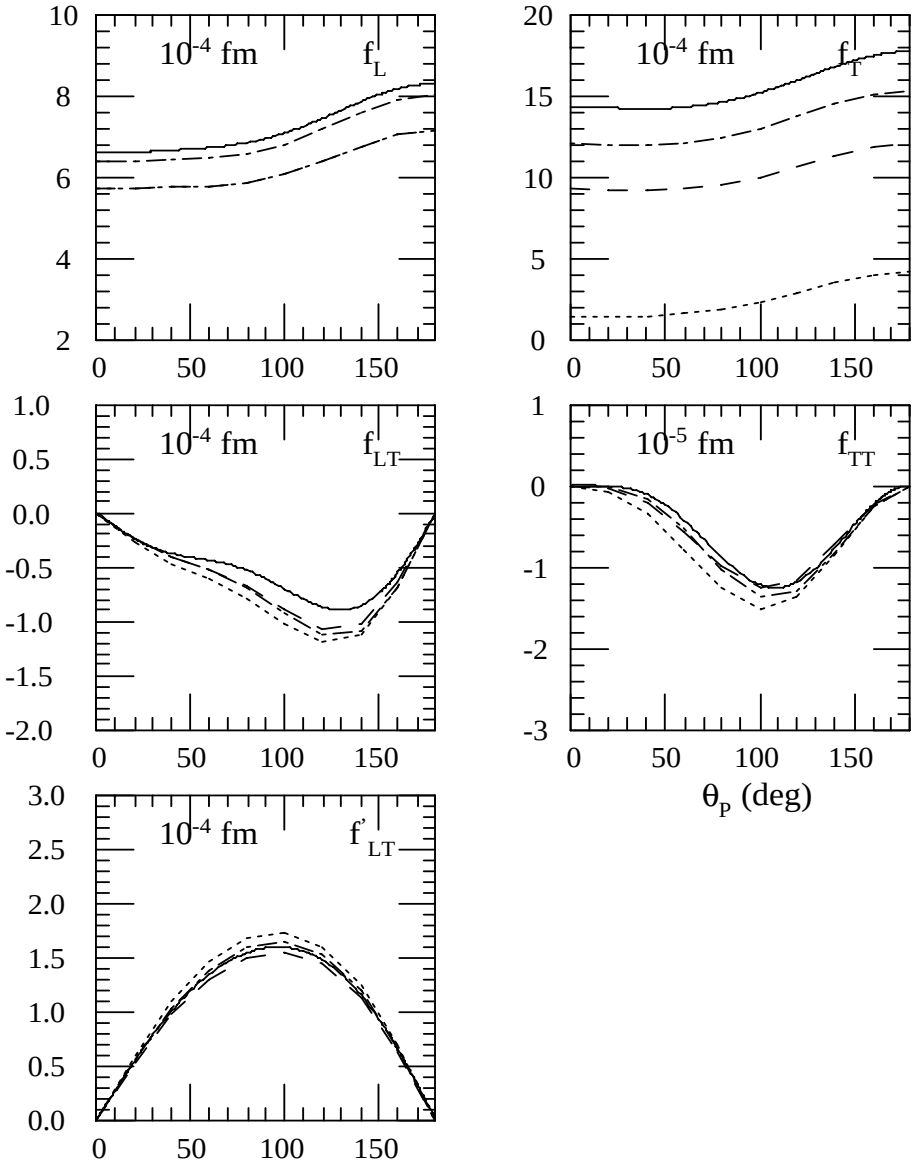

Figure 2: Theoretical structure functions for $Q^2 = 12fm^{-2}$ and $E_{np} = 2$ MeV. The dotted curve is for the Normal calculation; the dashed for Normal+MEC; the dash-dotted for Normal+MEC+IC; and the solid for Normal+MEC+IC+RC.

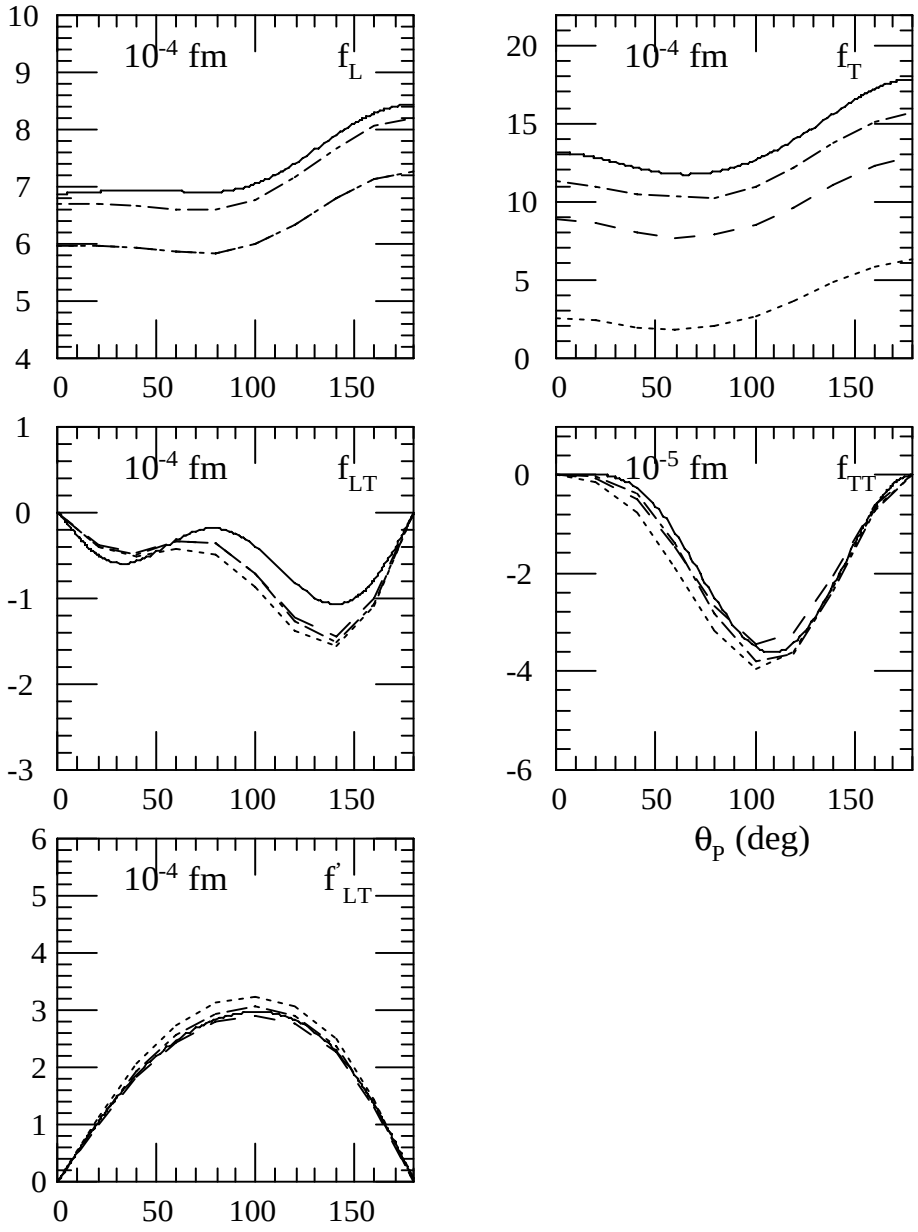

Figure 3: Theoretical structure functions for $Q^2 = 12fm^{-2}$ and $E_{np} = 4$ MeV. The dotted curve is for the Normal calculation; the dashed for Normal+MEC; the dash-dotted for Normal+MEC+IC; and the solid for Normal+MEC+IC+RC.

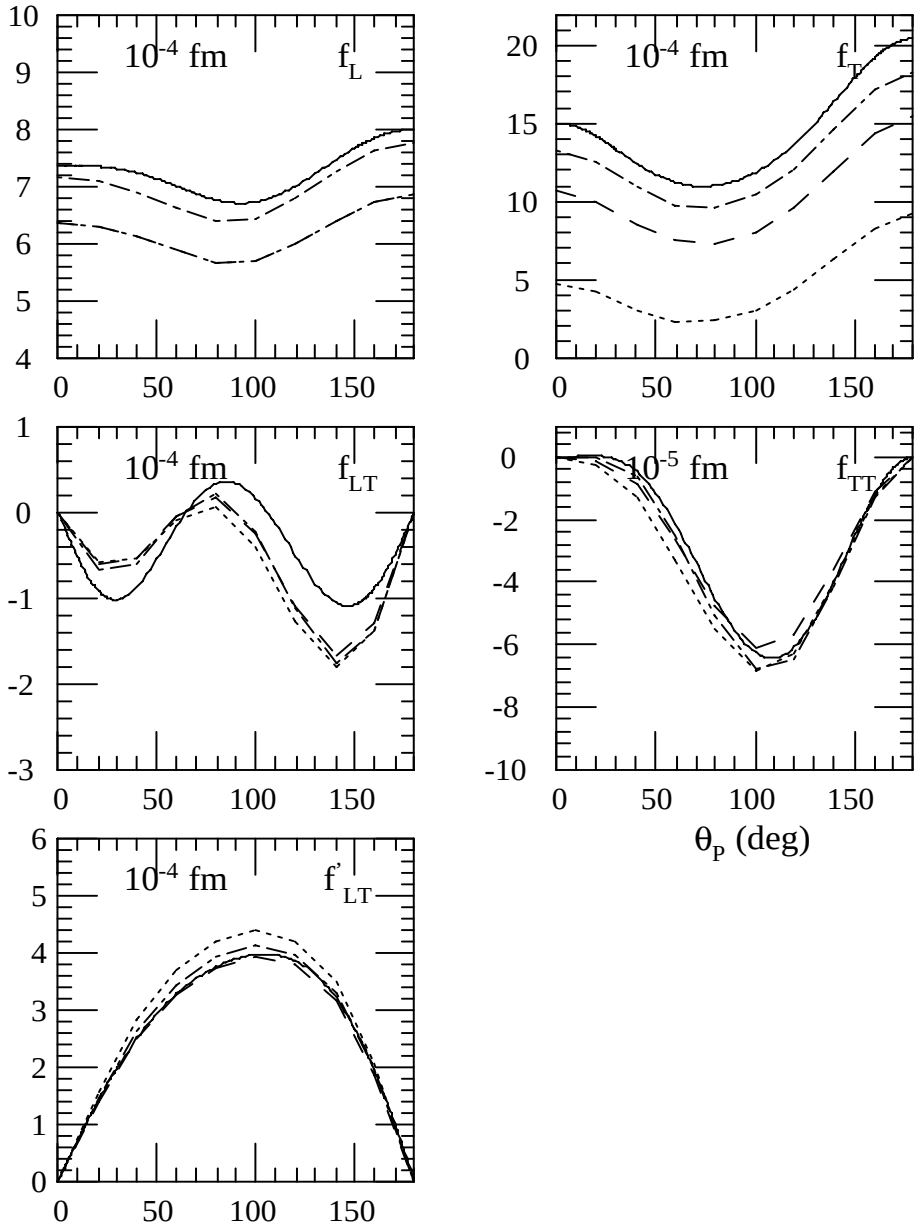

Figure 4: Theoretical structure functions for $Q^2 = 12fm^{-2}$ and $E_{np} = 6$ MeV. The dotted curve is for the Normal calculation; the dashed for Normal+MEC; the dash-dotted for Normal+MEC+IC; and the solid for Normal+MEC+IC+RC.

computed to have much effect on f_{TT}. However, if Arenhövel's calculations of this observable are reasonably accurate then the amplitude of f_{TT} will be an order of magnitude smaller than that of f_{LT}. Consequently, the error bars for f_{TT} are expected to be larger. It may, nevertheless, be possible to determine the amplitude of this term even if we cannot determine its shape with any precision.

To extract the fifth structure function f'_{LT}, one has to use a polarized electron beam. Since f'_{LT} originates from the imaginary part of the interference between the longitudinal and transverse components, it vanishes in a plane wave calculation as shown in [40]. Therefore, f'_{LT} data will be a direct measure of FSI, or the rescattering between the two nucleons.

While the details of the above discussion are specific to the calculation of Arenhövel general conclusions can be drawn. First, the previous success of this calculation suggests that it will at least set the scale for the observables to be measured. This gives us confidence that the precision anticipated in the proposed measurements will be adequate to illuminate new physics. Second, the particular sensitivities of the various observables to contributions from the underlying physics derive not from specifics of any one calculation but from more general principles. Consequently, the complementarity of the proposed measurements of a set of observables promises, in a quasi-model independent way, to delineate these contributions.

4 Experiment

4.1 Experimental Objectives

The proposed experiment will measure all the five structure functions at four values of E_{np} simultaneously. The three interference terms will be obtained over five Q^2 regions from 10 to 14 fm^{-2}. Due to the selective sensitivity, different physics will be focused on each structure function.

With f_L we will focus on the isovector charge current and IC effects; with f_T we will focus on the MEC effects; with f_{LT} we will focus on the RC effects; and with f'_{LT} we will focus on FSI. The function f_{TT} will be used as a check, albeit probably weak, of the Normal component of the calculations. To the degree permitted by our determination of the IC and RC contributions we will investigate the isovector charge currents via the f_L structure function.

We will employ one HRS to detect the scattered electrons and the BigBite spectrometer to detect the recoiling protons. The high resolution of the HRS will allow a precise determination of the ν and $\vec{q_3}$. The large acceptance of the BigBite will subtend a large fraction of the forward-emitted protons along $\vec{q_3}$. The Hall-A standard 15 cm long liquid deuteron target will be replaced by a 10 cm cell with thinner windows and walls. The other HRS will be utilized as a luminosity monitor during data acquisition.

4.2 BigBite and HRS Spectrometers

The new detector which makes this experiment feasible is the non-focusing BigBite spectrometer with its large solid angle (96 msr) and large momentum bite (200-900 MeV/c). The important parameters of this device are given in Table 2. The BigBite spectrometer was originally designed and constructed at NIKHEF to detect electrons [41, 42]. Its central element is a non-focusing dipole magnet. Funds are currently being requested for the construction of a new detector system consisting of two three-plane MWPCs and fast scintillator planes with which accurate timing (σ=0.75 ns) will be obtained.

The tracking information will obtained from the two MWPCs.

The two multi-wire proportional chambers will have an active area of 1400×350 mm^2 and 2000×500 mm^2 respectively and will contain 5000 sense wires in total. The sense wires in the two chambers are separated by 4.5 mm and 5.5 mm, respectively. One plane of wires will be tilted at 45°, a second at 135°, and the third will be oriented horizontally. The new chambers will improve the readout frequency from 27 kHz to a few MHz. It will therefore be possible to run the experiment at high luminosity up to a few $\times 10^{37}/s/cm^2$, since the total singles rate in BigBite will be approximately 3×10^6 Hz [43].

In addition to the counting rate being improved, the angular and momentum resolution will be improved by removing almost all material between the target cell and the detector so as to reduce straggling and multiple scattering.

	HRS	BigBite
p-range (MeV/c)	300-4000	200-900
acceptance_H (mrad)	±20	±80
acceptance_V (mrad)	±60	±300
solid angle (msr)	4.8	96
δ p/p	10^{-4}	5×10^{-3}
$\delta\theta_H$ (mrad)	0.6	3.2
$\delta\theta_V$ (mrad)	2.0	3.2
measure	$\vec{p}_e$, vertex	$\vec{p}_p$,vertex
σ_{vertex} (cm)	0.064	0.32
focusing	$< x\|\theta >= 0$	none

Table 2: Comparison of HRS and BigBite.

The Left-HRS (LHRS) spectrometer will be used to detect electrons. Its important parameters are summarized in Table 2. The LHRS will also be vacuum-coupled to the scattering chamber, again to reduce multiple scattering and straggling and to enable us to define the momentum transfer vector as precisely as possible.

4.3 Kinematics

To separate the transverse (f_T) from the longitudinal (f_L) components, we need to take data at two different ($E - \theta_e$) settings while Q^2 and E_{np} are kept constant; we change only the value of ϵ_L. The two longitudinal polarizations must differ by a sizable amount but the direction of $\vec{q}$ (the direction of the BigBite) cannot be too far forward or the singles rates will become too high. With the above considerations in mind, we chose (3200 MeV, 12.5°) and (550 MeV, 90.0°). Table 3 lists the major kinematic parameters for these settings, where θ_R is the recoil angle determined by the virtual photon direction, and the relative longitudinal polarization ϵ_L is obtained by Eq. 2.

E (MeV)	θ_e (HRS) (deg.)	Q^2 (fm^{-2})	θ_R (BB) (deg.)	ϵ_L
3200	12.5	12.0	72.8	0.976
550	90.0	12.0	37.3	0.344

Table 3: Kinematic conditions for L/T separation.

The overlap between the finite acceptances of the two spectrometers defines the kinematic space to be covered by the proposed measurements. Fig. 5 shows the covered region for each of the two kinematic conditions *as defined by the HRS*. The area bounded by the solid line is the region covered in the higher energy (3200 MeV, 12.5°) measurements while the area bounded by the combination of dotted and solid lines is the region covered in the lower energy (550 MeV, 90.0°) measurements. The complete 6-dimensional acceptance of the two spectrometer configuration is, of course, more complicated and will depend upon the placement of the BigBite spectrometer. This figure does, however, illustrate the relative acceptances of the forward and backward angle configurations.

The interference terms will be extracted from the high energy setting due to the larger cross sections. Consequently, these terms will be sampling a larger Q^2 range.

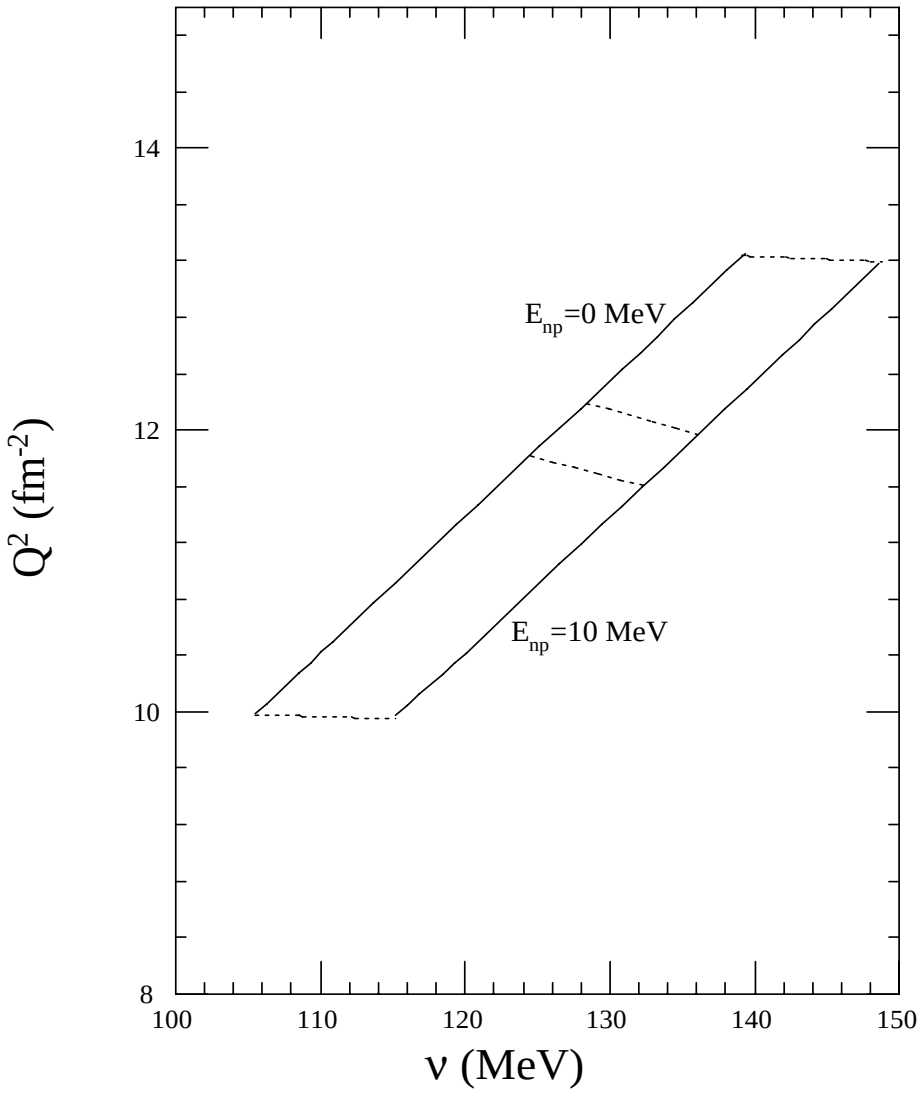

Figure 5: $Q^2 - \nu$ phase space coverage as defined by the HRS. The area bounded by the solid line is the region covered in the higher energy (3200 MeV, 12.5°) measurements while the area bounded by the combination of dashed and solid lines is the region covered in the lower energy (550 MeV, 90.0°) measurements.

Fig. 6 shows the dependence of the kinetic energy of the proton on the laboratory angle θ_q of the proton relative to the virtual photon direction at $Q^2 = 12fm^{-2}$. The radially dashed curves represent the CM polar angle θ_p, ranging from 10° to 170° clockwise. The most energetic protons are emitted at a CM angle of $\theta_p = 0°$; for $E_{np} = 8\ MeV$ they have a kinetic energy of 98 MeV, corresponding to a momentum of 440 MeV/c. The corresponding least energetic proton (for θ_p=180° in the CM frame) has an energy of 35 MeV and is also emitted at $\theta_q = 0°$. These momenta easily fall within the acceptance of the BigBite spectrometer.

If the BigBite spectrometer is centered on the nominal direction of $\vec{q}$ then only protons emitted at θ_p from 0° to 5° and from 140° to 180° will be detected when $E_{np} = 2\ MeV$. However, if two spectrometer positions are used for each HRS setting and the running time divided between the two configurations, then data will be taken for all values of θ_p and ϕ_p up to $E_{np} = 4MeV$ at $Q^2 = 12fm^{-2}$. We therefore plan to take data with the BigBite positioned along either side of the nominal direction of $\vec{q}$ for each of the two HRS settings.

4.4 Calibration of BigBite

The electromagnetic calorimeter (EC) designed for experiment E99-114 [44] in Hall-A will be used in the calibration of the acceptance of BigBite spectrometer. It will measure the energy and angle of electrons scattered elastically from the proton while the BigBite will detect the recoiling proton. The energy and spatial resolution of the scattered electron can be determined with an energy resolution better than $\sigma_{\delta E/E} = 0.01 + 0.06/\sqrt{E(GeV)}$ and a spatial resolution of 4.3 mm. Positioning the calorimeter with an accuracy of 1 mm will allow an absolute angular calibration of the BigBite spectrometer to accuracy of 0.2 mrad.

The Hall A multi-foil target will be used to calibrate the vertex reconstruction of the target position. The thin CH_2 target and the 10 cm liquid hydrogen

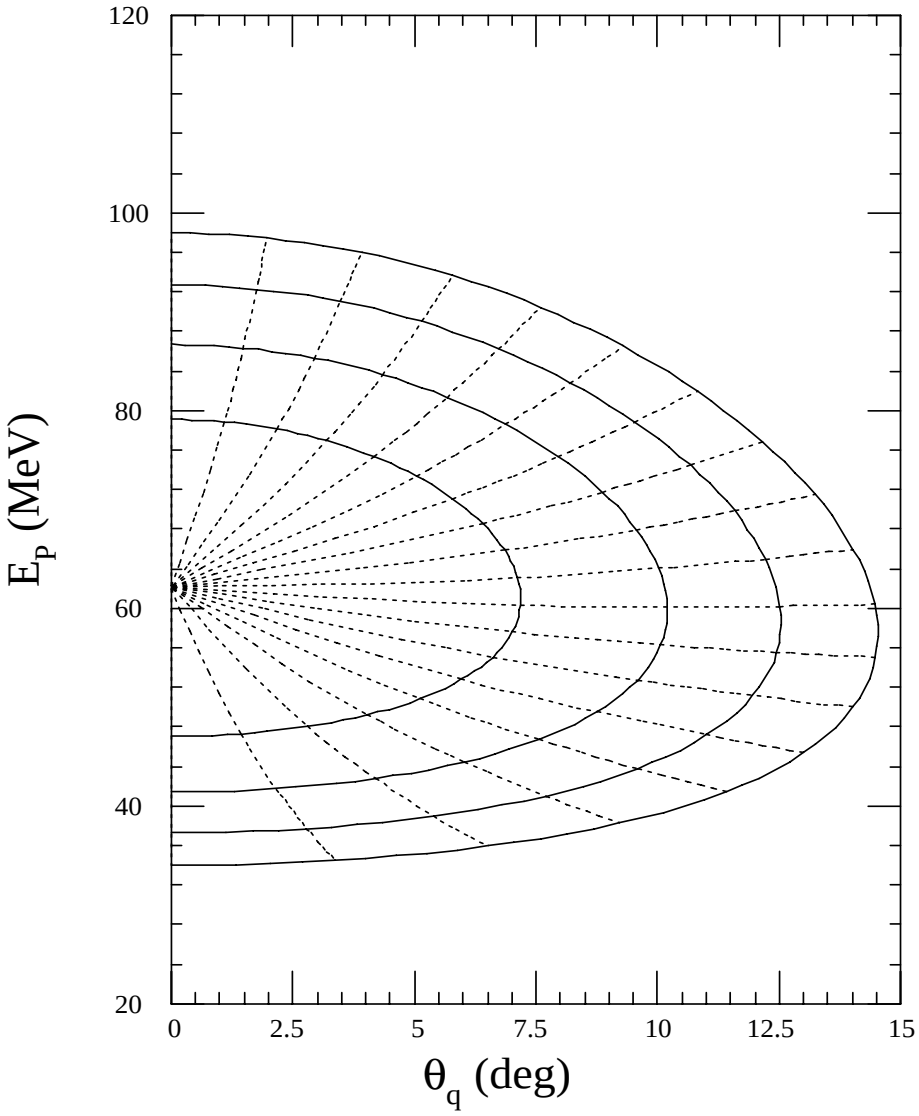

Figure 6: Proton kinetic energy dependence on the polar angle relative to the virtual photon in the laboratory system for Q^2=12 fm^{-2} and E_{np}= 2 MeV to 8 MeV. The dashed curves label the CM polar angle of the proton from 10° to 170°.

target will be used during the calibration. Due to the large momentum acceptance of the BigBite spectrometer, we will use the elastic radiative tail to calibrate the entire momentum acceptance with a minimum number of beam energies. This calibration will provide the momentum precision to better than 0.5%, and a recoil angle precision better than 1 mrad. The techniques to be used are similar to those developed at NIKHEF and will follow the methods under development for the previously approved threshold π^0 electro-production experiment [43].

Near threshold, the momenta of deuterons recoiling from an elastic scattering event will be twice those of protons from disintegration. These recoiling deuterons can be used as an online calibration of the BigBite detector since they can easily be separated from the protons by either time-of-flight (TOF) or E-dE/dx characteristics.

4.5 Luminosity Measurement

The target thickness-beam current product will be determined with accuracy of about 1-2 %, sufficient for the proposed experiment, by measuring elastic scattering. The relative luminosity during the measurements will be monitored in the RHRS to better than 1%. This technique of using elastic scattering followed by continuous luminosity monitoring has been used by the Hall A E89-044 and E97-111 experiments.

4.6 Target Cell

The standard Hall A 15 cm long, liquid deuterium target cell will be replaced by a 10 cm cell with thinner entrance and exit windows and side walls. This is necessary to reduce straggling and multiple scattering for the low energy protons. The existing cryogenic system will be used without modification. The side walls of the cell will be 25 μm thick; the entrance and exit windows will be 15 μm thick. The parameters of target cell are listed in Table 4.

Density	0.162 gm/cm^3
Cell Length	10.0 cm
Cell Diameter	1.0 cm
Cell Material	Al
Entrance window	0.0015 cm
Exit window	0.0015 cm
Side wall	0.0025 cm

Table 4: The liquid deuterium target cell parameters.

5 Experimental Simulation

5.1 Resolution

The major kinematic variables such as Q^2, W, θ_e, and hence E_{np} are determined by the electron arm. The direction of $\vec{q}$ to which the direction of the proton is referenced is also determined from these quantities. The resolution inherent in determining the quantities of physical interest were obtained by propagating the uncertainties in the direct observables, $\sigma_E/E = 0.0002$, $\sigma_{E'}/E' = 0.0001$, $\sigma_{\theta_e} = 2mrad$. One of our major concerns is the precision of the invariant mass W, which is better in the lower energy and backward angle configuration. In a compromise for the two settings we chose a bin size for E_{np} of 2 MeV.

A GEANT simulation was performed to determine the resolution of the detector system based on a code written by Vladimir Nelyubin [43]. The following results were obtained with a beam energy of 3200 MeV, the HRS located at 12.5°, and the BigBite located at 72.8°. The excitation energy E_{np} was spread from 0 to 10 MeV. Fig. 7 shows the resolution of Q^2, E_{np} and the missing mass of the neutron. Fig. 8 shows the resolution of the polar and azimuthal angle of the proton in the CM system. With the projected angular resolution, it is feasible to choose a bin size of 10° for both θ_p and ϕ_p.

5.2 Acceptance

To perform a Monte Carlo study of the acceptance of the BigBite spectrometer, an event generator was prepared to provide events uniformly distributed in the θ_p-ϕ_p plane in the center mass system for a fixed beam energy, a given electron scattering angle, and an invariant mass W. The events were then processed by the aforementioned Monte Carlo code. Fig. 9 shows the 2-dimensional acceptance distribution for the proton at $E_{np} = 2$ MeV and Q^2=12 fm^{-2} in two BigBite settings.

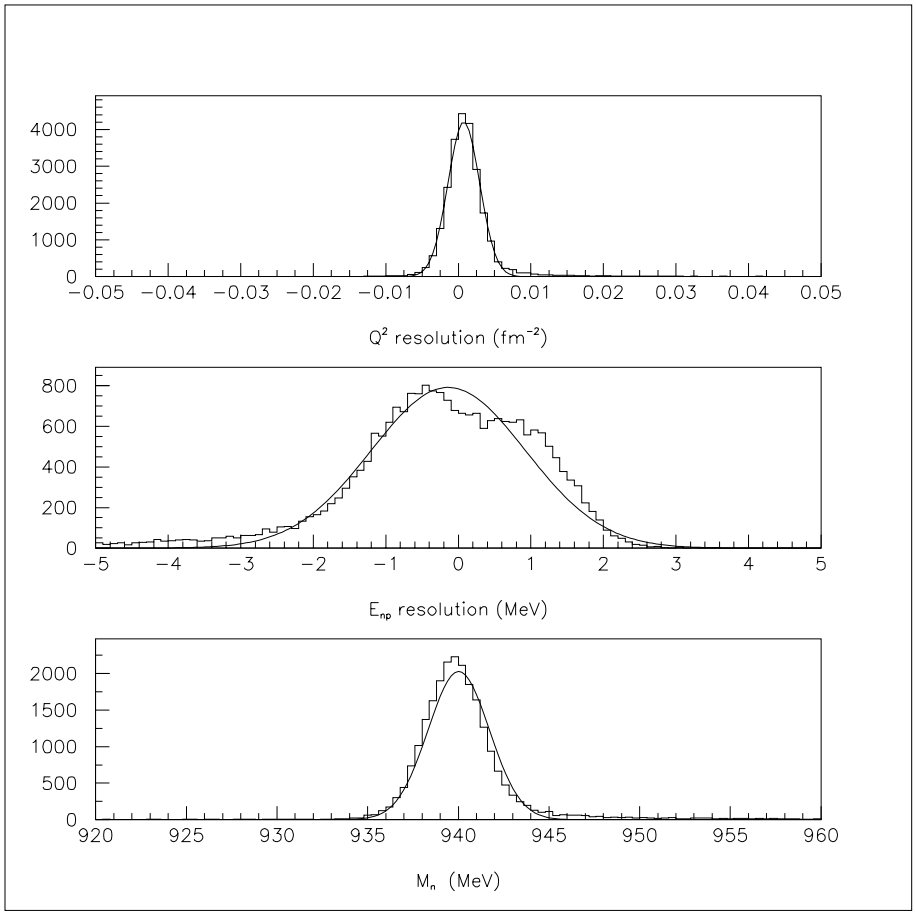

Figure 7: Resolution of Q^2, E_{np} and the missing mass.

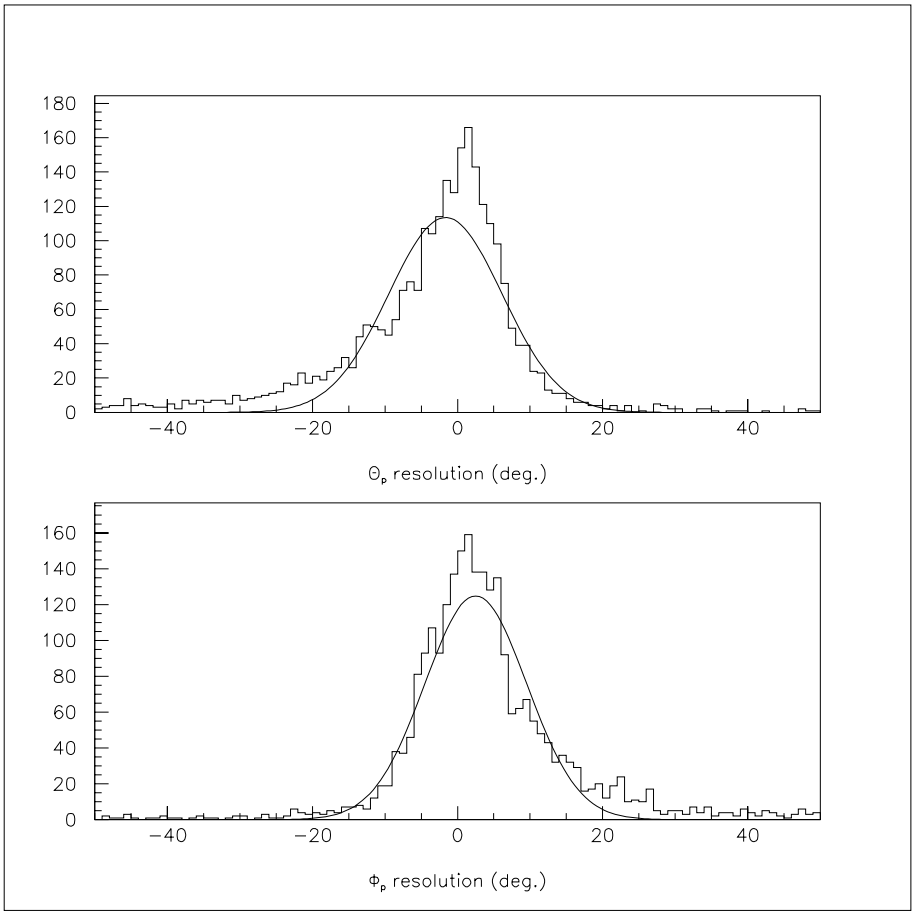

Figure 8: Resolution of θ_p, ϕ_p in CM system.

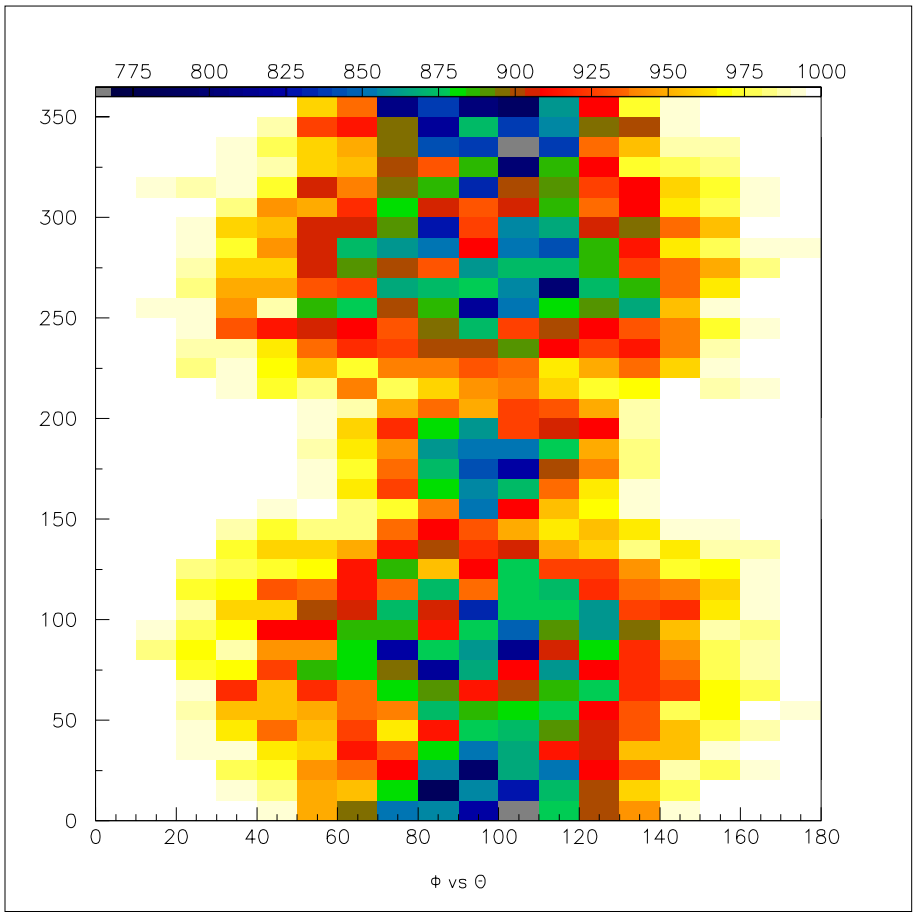

Figure 9: Acceptance distribution for the proton arm at $E_{np} = 2$ MeV and Q^2=12 fm^{-2}.

5.3 Systematic Uncertainties

Under the heading of systematic or non-statistical uncertainties we include four groups. First, there are uncertainties in our knowledge of the acceptance of the BigBite spectrometer. Since this will be measured *in situ* and will be continuously monitored we estimate that it will introduce only about a 2% "acceptance" uncertainty; less for low values of E_{np}, somewhat more for high values of E_{np}. Second, there are the effects of the finite momentum and angular resolutions of the HRS. Because the cross sections are strong functions of both electron energy and angle these can cause a "skewing" of the results. In principle, these effects can be removed but we have not investigated the degree to which this is possible so we assumed that we could remove only 50% of their effect. We list them as a "resolution" uncertainty. In our calculations we assumed FWHM values of 1×10^{-4} for $\delta E'/E'$ and 2 mrad for $\delta\theta_e$. Third, there is the uncertainty in our knowledge of the beam current and target thickness. These combine to produce a "normalization" uncertainty of 2%. One would hope that any systematic error in the beam current and target thickness would be the same for both the forward and backward angle data. However, in determining the effects of this "normalization" uncertainty in our extraction of f_L and f_T we have conservatively assumed that the two data sets have statistically independent "normalization" uncertainties and have added their effects in quadrature. Fourth, there are the "absolute" uncertainties associated with our absolute knowledge of the electron beam energy, δE_e $(=2 \times 10^{-4})$ and of the central angle of the HRS, $\delta\theta_{HRS}$ (=0.2 mrad).

Significantly, uncertainties in the positioning and absolute momentum setting of the BigBite spectrometer have not been listed. This is because we will determine these parameters using the same technique used to calibrate 180° electron scattering systems at the MIT-Bates Laboratory and elsewhere. We will select electron events in the HRS for which the direction of $\vec{q}$ is the same but for which E_{np} ranges from 0 MeV to some finite value. The phase space factors in Eq. 1 make the cross section rise quickly as E_{np} increases from

0 MeV, independent (for small E_{np}) of azimuthal angle. Consequently, the distribution of protons as a function of the angle between their momenta and $\vec{q}$ will be a parabola centered on $\vec{q}$. Similarly their energies will be distributed in a predictable pattern about a value calculable from the electron kinematics. The error in the calibration of the direction of $\vec{q}$ was estimated by simulating a representative distribution of protons generated by monochromatic electrons scattering (nominally) through a fixed angle with a fixed energy loss; the actual scattering angle and energy loss were varued according to the HRS resolutions. A simple fit of the andle and momenta of the recoiling protons yielded a measure of the $\vec{q}$ direction within about 0.3 mrad, a little more than the electron energy or angle. Thus, as in the case of 180° electron scattering we will use the data to calibrate the data.

In evaluating the effects of systematic or non-statistical uncertainties upon the extracted quantities one must note that 1) the dependence of the determinations of the interference structure functions, f_{LT}, f_{TT},and f'_{LT}, on systematic uncertainties differs greatly from that of the Rosenbluth extraction of f_L and f_T and 2) that the direction of $\vec{q}$ is determined solely by the electron kinematics. Since the interference structure functions, f_{LT}, f_{TT}, and f'_{LT} are determined from the distribution of protons about $\vec{q}$ the systematic uncertainties associated with them come mainly from the multiplicative acceptance and normalization uncertainties. These combine to give a systematic uncertainty of about 4%. For the longitudinal and transverse structure functions extracted from a Rosenbluth separation, the effects of the systematic uncertainties were determined by applying them separately to each of the forward and backward angle measurements and then extracting f_L and f_T. The results of this calculation are shown in table 5.

5.4 Backgrounds and Accidental Coincidences

The kinematics of the proposed measurements involve the highest energy scattered electrons possible from a deuterium target. Consequently, there is no other single process that can generate an (e,p) or (e,d) coincidence that could be mistaken for an event of interest. Figure 10 shows, for measurements at (3200 MeV, 12.5°) the distribution of electron energies versus scattering

	Resolution (%)	Normalization (%)	Absolute (%)
δf_L	2.1	5.3	1.0
δf_T	2.8	5.7	1.0

Table 5: Effects of systematic uncertainties in the Rosenbluth separation of f_L and f_T.

angle within the HRS acceptance for the first three processes: elastic scattering, electrodisintegration (E_{np} = 0 MeV and 10 MeV), and quasielastic scattering. The cross sections for these three processes under these kinematics are

p elastic	$\approx 1 \times 10^{-30}$	cm^2/sr
d elastic	$\approx 2 \times 10^{-33}$	cm^2/sr
d electrodisintegration	$\approx 1 \times 10^{-33}$	cm^2/sr (depends on E_{np}^{max})

Thus, the counting rate in the HRS for quasi-elastic scattering will dominate by a factor greater than 300 the rates of the other processes. We plan, therefore, to place before the HRS detector an additional scintillator plane. The scintillators will cover the upper (lower electron energy) region of the focal plane with its lower edge angled so that electrons with energies below the indicated dashed line in fig. 10 will trigger it. Such events will be prescaled by a factor to be determined at the time of running.

Accidental coincidences between products of different reaction events are a significant concern. While the electrons corresponding to events of interest all fall near the upper end of the energy range, positively charged particles with a wide variety of momenta can be of interest. Protons from quasi-elastic scattering and/or pion production as well as pions will be detected in the BigBite spectrometer.

The experimental conditions proposed for the forward angle ($E_e = 3200$ MeV, $\theta_e = 12.5^\circ$) measurements correspond to a singles rate of not more than 3 MHz in the BigBite spectrometer and about 1 MHz in the HRS [45]. It

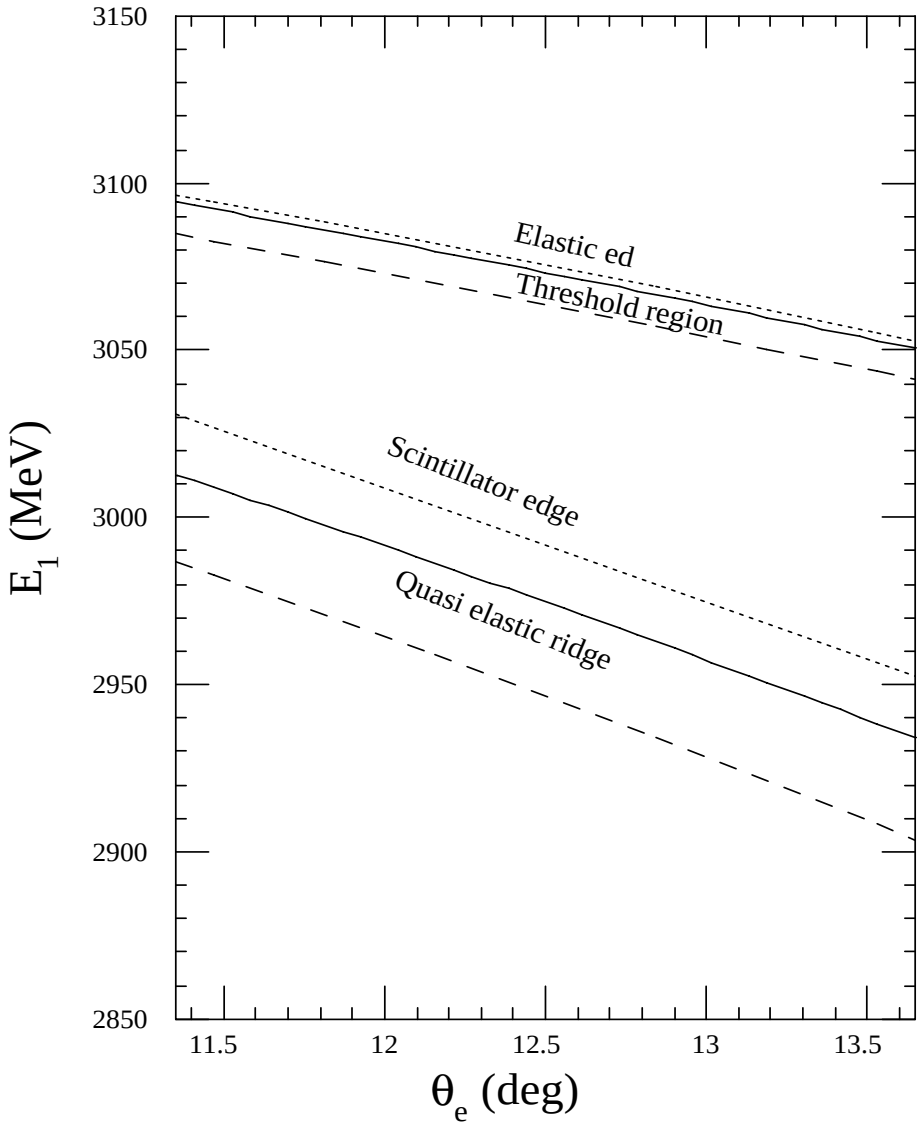

Figure 10: Distribution of electrons on the HRS focal plane. Electrons from elastic (upper short-dashed line) and threshold electrodisintegration events (upper solid line - $E_{np} = 0$ MeV, upper long-dashed line - $E_{np} = 10$ MeV) are clearly separated from from those coming from quasi-elastic events. The lower long-dashed (solid) line indicates the electron energy corresponding to a scattering from a proton with initial momentum equal to the Fermi momentum anti-parallel (parallel) to $\vec{q}$. A plane of scintillator with its lower edge (corresponding to higher energy) as indicated by the short-dashed line will enable us to reduce the singles rate in the HRS by prescaling events in which an electron strikes this scintillator.

should be noted that when compared to measurements made using a proton target this calculation overestimated the flux of protons by a factor of about 2. [46] Thus, our use of this number must be considered conservative. After prescaling the quasi-elastic, Δ, etc. electrons by a factor of 300 the remaining rate in the HRS will be not more than 4 kHz. With a coincidence window of 40 ns, one obtains an accidental coincidence rate of about 500 Hz, well within the capabilities of the data acquisition system. The rates for the backward angle measurements will be much lower so it may be possible to reduce the prescale factor and increase the data obtained on the quasi-elastic scattering process.

5.5 Rate Estimate

To get an estimate of the precision in the final observable, we use the cross section formulas in Eq. 1 and the full calculation from Arenhövel at $E_{np} = 2$ MeV as shown in Fig. 2. The estimate is based on a 10 cm long deuterium target and 10 μA beam current. The solid angle of the HRS is taken to be 5 msr and the bin size of θ_p and ϕ_p is 10°. Table 6 lists the estimated rates for $E_{np} = 2 \pm 1$ MeV.

E (MeV)	θ_e (deg.)	Q^2 (fm^{-2})	$\frac{d\sigma}{d\Omega_e dW}$ (fm^2/sr/MeV)	rate (1/s)
3200	12.5	12.0	3.96×10^{-8}	144
550	90.0	12.0	1.04×10^{-9}	3.8

Table 6: Rate estimate for each HRS setting and $E_{np} = 2 \pm 1$ MeV.

The high energy, forward angle setting covers a larger kinematic region. Hence, the effective counting rate for data useful in the L/T should be divided by about five. For 10° bins of θ_p and ϕ_p, we will have 648 2-dimensional (one for each electron helicity) cells. Table 7 lists the tentative beam time and anticipated total counts for 120 hours of running. Since the BigBite will have two placements for each HRS setting, the total beam time will be twice

this. We therefore request 20 days of beam time for the measurements themselves. Including five days for calibration and detector set up, we request 25 days in total for the measurement.

For a 10-day run at high energy with two BigBite settings, approximately 5.6×10^6 events will be accumulated in each 2 MeV E_{np} bin and 0.37 fm^{-2} Q^2 bin. The average statistical precision for each cell will be about 1%. For a 10-day run at lower energy and larger angle with two BigBite settings, approximately 1.6×10^6 events will be accumulated in each E_{np} bin. The average statistical precision for each cell will be about 2%. This will make it possible to perform the L/T separation with a statistical precision of 3-5%.

E (MeV)	θ_e (deg.)	rate $(1/s)$	beam time (hour)	counts (M)
3200	12.5	13	120	5.6
550	90.0	3.8	120	1.6

Table 7: Beam time and data totals for 2 MeV bins in E_{np}, 0.37 fm^{-2} bin for Q^2, and 10° bin for both θ_p and ϕ_p.

We will also collect approximately 100×10^6 (2×10^6) deuteron elastic events during the higher (lower) energy run. This large number of kinematically overdetermined events will be useful as a means of on-line calibration.

5.6 Projected Results

Using the full (Normal+MEC+IC+RC) calculation of Arenhövel as the generating function the experiment was simulated. The interference structure functions were extracted using the data from the entire range of Q^2 measured at 12.5° (41 M events). The longitudinal and transverse structure functions were extracted using the data from the restricted range of Q^2 measured at both 12.5° and 90°. Figure 11 shows the simulated data for f_{LT} atop the calculation of Arenhövel. The error bars are statistical only; the systematic

uncertainty is approximately equal to the statistical.

Figure 12 shows the simulated data for f_{TT} and f'_{LT} atop the calculation of Arenhövel. The error bars are statistical only; the systematic uncertainty is smaller than the statistical. In this figure the data have been grouped into 20° rather than 10° bins.

To simulate the separation of the longitudinal from the transverse structure functions, we have used 5.6 M events from 3200 MeV, and 1.6 M events from 550 MeV, since the Q^2 range is limited by the low energy set up. Figure 13 shows the simulated f_T and f_L atop the calculation of Arenhövel. The error bars are statistical only; the systematic uncertainty is smaller than the statistical and is indicated on the figure.

In general, with 5.6×10^6 events from the high energy run and 1.6×10^6 events from low energy run, we will determine f_L and f_T with very good precision. We will also determine f'_{LT} with good precision but can expect to extract little information from f_{TT}. The data from this experiment will be the first comprehensive set of high quality measurements of threshold deuteron electrodisintegration under kinematic conditions where non-nucleonic degrees of freedom are expected to play major roles. The selectivity of the different structure functions to each non-nucleonic effect provides a powerful tool to focus on each component.

These data will be precise enough to study the isovector charge current and IC contributions to f_L, the MEC contributions to f_T, and the relativistic effects in f_{LT}. These high quality data will put stringent constraints on theoretical models and lay a solid foundation for extending the studies to higher momentum transfers. The data on f'_{LT} will provide a meaningful check on the impulse approximation and the final state interactions since they are expected to be insensitive to IC, MEC and the relativistic effects.

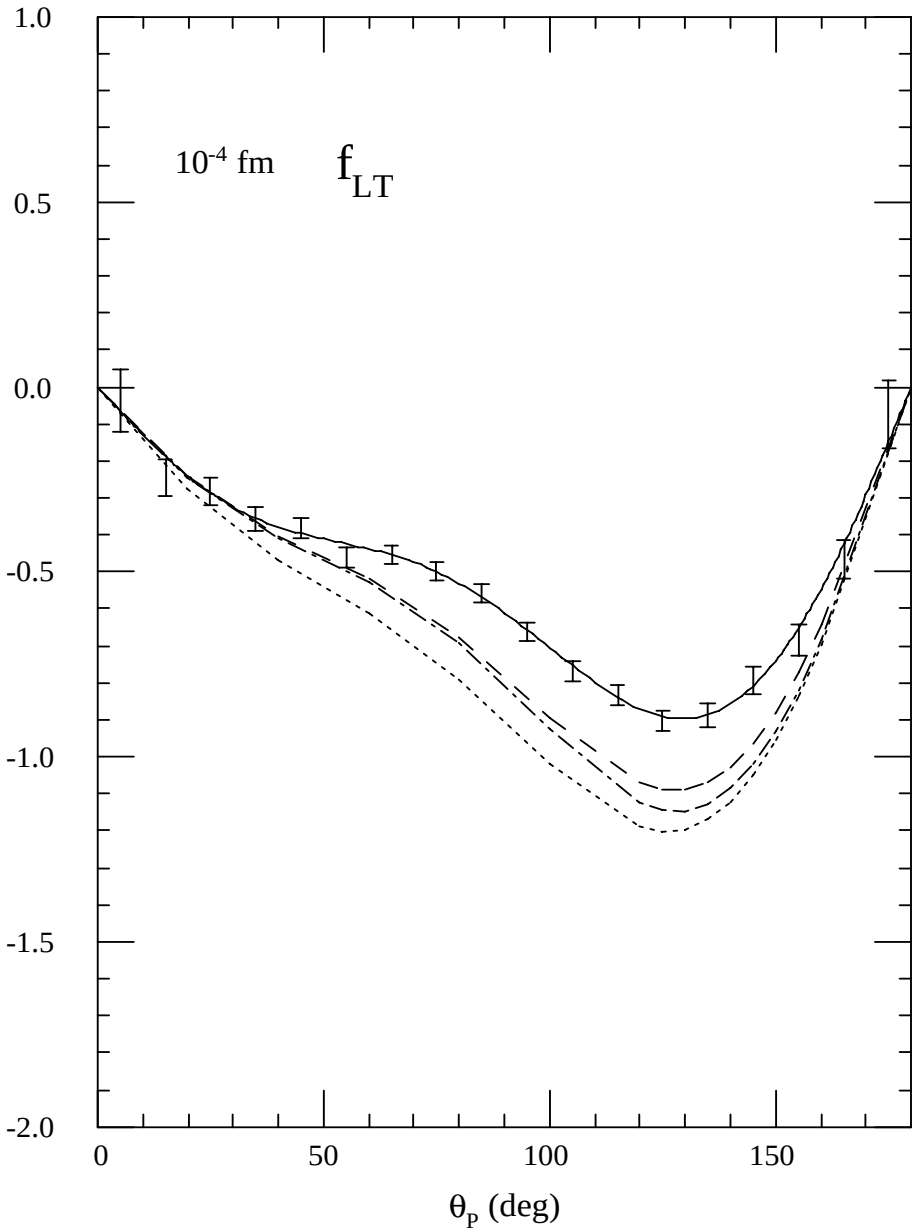

Figure 11: Simulated data for Q^2=12 fm^{-2} and E_{np} = 2 MeV. The dotted curve represents the Normal calculation, the dashed curve represents the Normal+MEC, the dash-dotted represents the Normal+MEC+IC, and the solid curve represents the Normal+MEC+IC+RC calculation. The data span the range in Q^2 from 10 fm^{-2} to 13.2 fm^{-2}

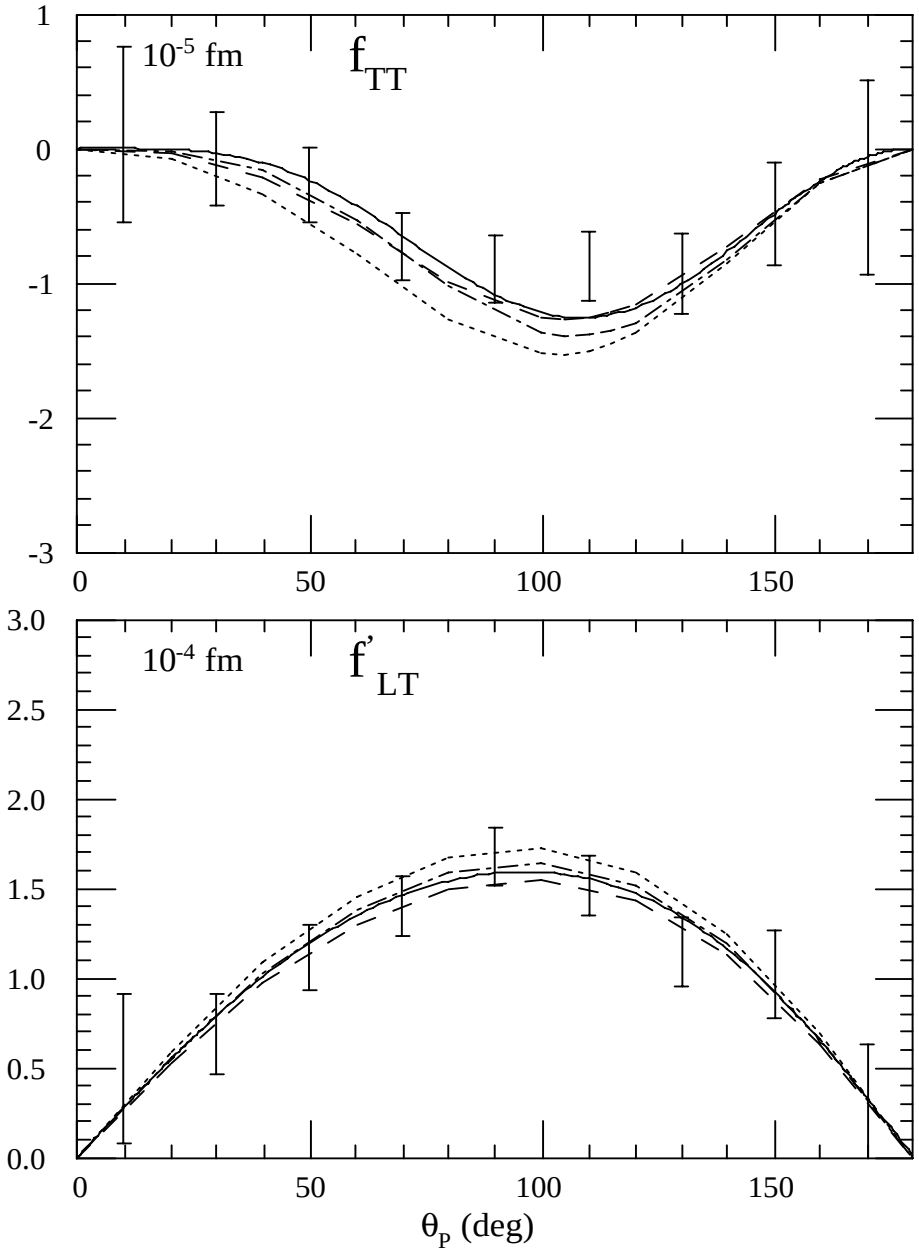

Figure 12: Simulated data for Q^2=12 fm^{-2} and E_{np} = 2 MeV. The dotted curve represents the Normal calculation, the dashed curve represents the Normal+MEC, the dash-dotted represents the Normal+MEC+IC, and the solid curve represents the Normal+MEC+IC+RC calculation. The data span the range in Q^2 from 10 fm^{-2} to 13.2 fm^{-2}

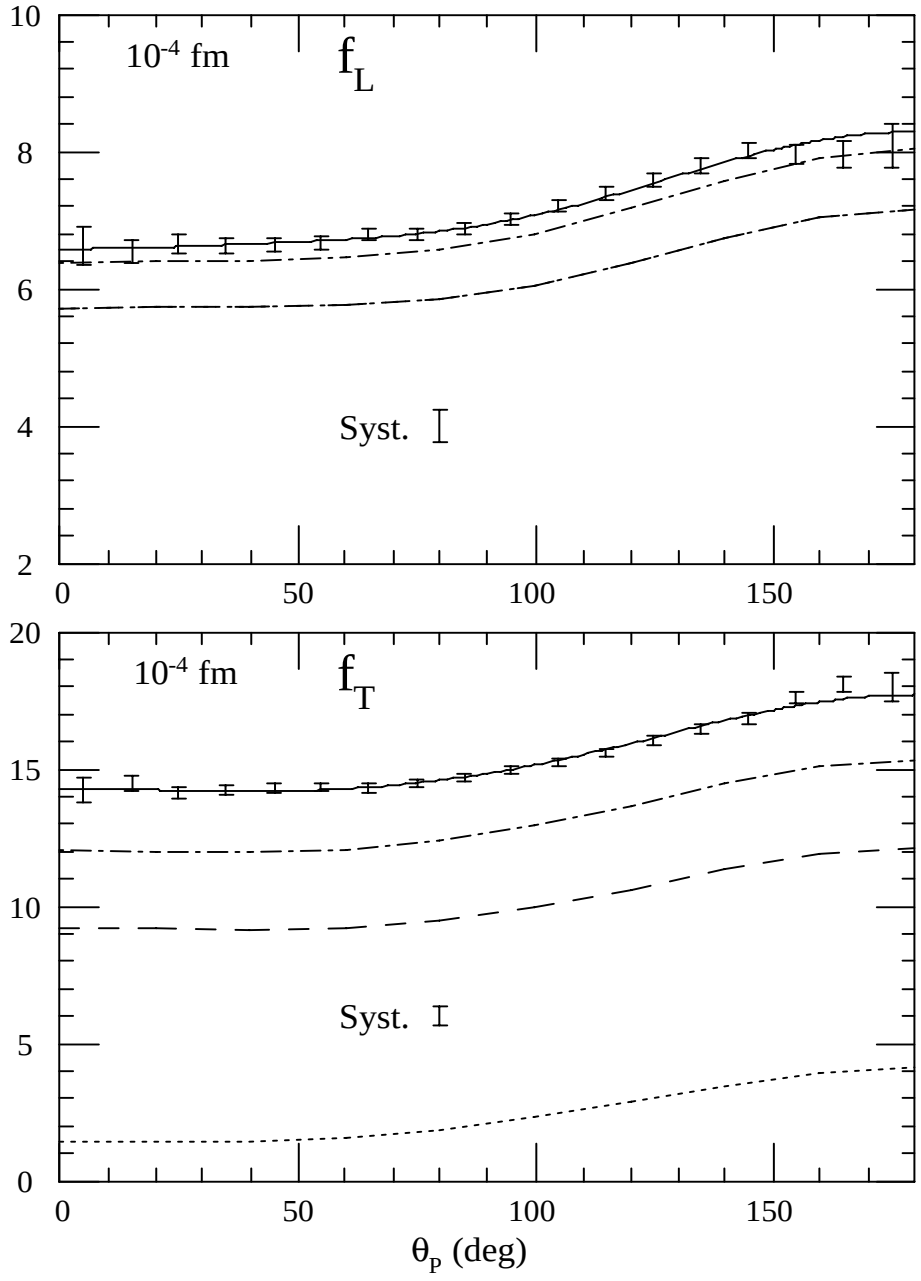

Figure 13: Simulated data for Q^2=12 fm^{-2} and E_{np} = 2 MeV. The dotted curve represents the Normal calculation, the dashed curve represents the Normal+MEC, the dash-dotted represents the Normal+MEC+IC, and the solid curve represents the Normal+MEC+IC+RC calculation. The data span the range in Q^2 from 11.78 fm^{-2} to 12.15 fm^{-2}

5.7 Beam Time Request

Table 8 lists beam time distribution for each kinematic condition. θ_{HRS} and θ_{BB} are the orientation angles of the HRS and BigBite spectrometers respectively. The data from part I will provide the three interference structure functions, as well as the sum of the net transverse and longitudinal part in five Q^2 bins. The purpose of the part II run is to make possible a Rosenbluth separation of f_L and f_T.

	E (MeV)	θ_{HRS} (deg.)	θ_{BB} (deg.)	time (day)
part I	3200	12.5	67.8	5
	3200	12.5	77.8	5
part II	550	90.0	32.3	5
part II	550	90.0	42.3	5
set up				5
total				25

Table 8: Beam time requested for each kinematic condition. The five days for set up include time for detector calibration and alignment.

6 Summary

We propose an exclusive study of the reaction $d(\vec{e}, e'p)n$ at $Q^2 = 12\ fm^{-2}$ and $E_{np} = 2$ to $8 MeV$ in Hall A with the HRS and BigBite spectrometers. We will simultaneously measure elastic scattering from the deuteron, detecting both the scattering electron and the recoil deuteron. We request 25 days of beam time, of which 20 days will be for data acquisition and 5 days for detector placement and calibration. This will be the first systematic measurement of near threshold electrodisintegration of the deuteron in out-of-plane kinematics at a momentum transfer Q^2 where non-nucleonic degrees of freedom are expected to play major roles.

Over the last 20^+ years unseparated differential cross section data on threshold deuteron electrodisintegration have constituted one of the primary benchmarks against which all nucleon-nucleon interaction calculations have been tested. The proposed measurements will yield data which will provide a new set of benchmarks against which nucleon-nucleon interaction calculations can be tested to a higher level.

References

[1] PAC 14 Few-Body Workshop, Willimasburg, July, 1998.

[2] S. Auffret *et al.*, Phys. Rev. Lett. **55**, 1362 (1985).

[3] B. Mosconi and P. Ricci, Nucl. Phys. **A517**, 483 (1990).

[4] F. Ritz, H. Goller, T. Wilbois, and H. Arenhövel, Phys. Rev. C **55**, 2214 (1997).

[5] G. van der Steenhoven *et al.*, in AIP Conf. Proc 243, P793, 1991.

[6] W. Kasdorp *et al.*, Phys. Lett. B **393**, 42 (1997).

[7] F. Frommberger *et al.*, Phys. Lett. B **339**, 17 (1994).

[8] H. Arenhövel, Few-Body Sys., Suppl **6**, 206 (1992).

[9] G. Peterson and W. Barer, Phys. Rev. **128**, 812 (1962).

[10] K. S. Lee *et al.*, Phys. Rev. Lett. **67**, 2634 (1991).

[11] W. Schmitt *et al.*, Phys. Rev. C **56**, 1687 (1997).

[12] Y. Antuf'ev *et al.*, Sov. J. Nucl. Phys. **22**, 121 (1976).

[13] V. Agranovich *et al.*, Sov. J. Nucl. Phys. **25**, 595 (1978).

[14] M. Bernheim *et al.*, Phys. Lett. **B142**, 145 (1984).

[15] T. Tamae *et al.*, Phys. Rev. Lett. **59**, 2919 (1987).

[16] T. Tamae, Proposal to MIT Bates, 1990, proposal to Bates, 1990, 89-15.

[17] T. Reichelt *et al.*, in AIP Conf. Proc 243, P794, 1990.

[18] S. Dolfini *et al.*, Phys. Rev. C **60**, 64622 (1999).

[19] Z.-L. Zhou *et al.*, Phys. Rev. Lett. **87**, 172301 (2001).

[20] M. van der Schaar *et al.*, Phys. Rev. Lett. **68**, 776 (1992).

[21] A. Pellegrino *et al.*, Phys. Rev. Lett. **78**, 4011 (1997).

[22] J. Ducret *et al.*, Phys. Rev. C **49**, 1783 (1994).

[23] B. Bodan *et al.*, Nucl. Phys. A **549**, 471 (1992).

[24] M. van der Schaar *et al.*, Phys. Rev. Lett. **66**, 2855 (1991).

[25] D. Jordan *et al.*, Phys. Rev. Lett. **76**, 1579 (1996).

[26] Z.-L. Zhou, PROC on the 2nd workshop on electronucleon physics with Int target, 1999.

[27] K. Blomquist *et al.*, Phys. Lett. B **424**, 33 (1998).

[28] R. Böhm, thesis, Mainz, 2001.

[29] H. Bulten *et al.*, Phys. Rev. Lett. **74**, 4775 (1995).

[30] R. Arnold *et al.*, Phys. Rev. Lett. **35**, 776 (1975).

[31] S. Auffret *et al.*, Phys. Rev. Lett. **54**, 649 (1985).

[32] W. Fabian and H. Arenhövel, Nucl. Phys. **A314**, 253 (1979).

[33] H. Arenhövel, Nucl. Phys. A **384**, 287 (1982).

[34] M. Bernheim *et al.*, Nucl. Phys. **A365**, 349 (1981).

[35] J. Laget, Phys. Lett. B **199**, 493 (1987).

[36] A. Cambi, B. Mosconi, and P. Ricci, Phys. Rev. Lett. **48**, 462 (1982).

[37] A. Cambi, B. Mosconi, and P. Ricci, Phys. Rev. C **26**, 2358 (1982).

[38] H. Arenhövel *et al.*, Phys. Rev. C **52**, 1232 (1995).

[39] E. Hummel and J. Tjon, Phys. Rev. C **49**, 21 (1994).

[40] H. Arenhövel, private communication, 2001.

[41] D. de Lange *et al.*, Nucl. Instr. and Meth. **A 406**, 182 (1998).

[42] D. de Lange *et al.*, Nucl. Instr. and Meth. **A 412**, 254 (1998).

[43] D. Lindgren *et al.*, Proposal to Jlab, 01-014, 2001, unpublished.

[44] C. Hyde-Wright *et al.*, proposal E99-114 to CEBAF (unpublished).

[45] P. Degtiarenko, private communication, 2001.

[46] R. Lindgren, private communication, 2001.